Journal of Virology

Virology | Full-Length Text

RUNX3 inhibits KSHV lytic replication by binding to the viral genome and repressing transcription

Pengyu Ren,[1] Danping Niu,[1] Sijia Chang,[1] Lei Yu,[1] Junrui Ren,[1] Yuanming Ma,[1] Ke Lan[1,2,3]

AUTHOR AFFILIATIONS See affiliation list on p. 19.

ABSTRACT Kaposi's sarcoma-associated herpesvirus (KSHV) belongs to the gamma herpesvirus family, which can cause human malignancies including Kaposi sarcoma, primary effusion lymphoma, and multicentric Castleman's diseases. KSHV typically maintains a persistent latent infection within the host. However, after exposure to intracellular or extracellular stimuli, KSHV lytic replication can be reactivated. The reactivation process of KSHV triggers the innate immune response to limit viral replication. Here, we found that the transcriptional regulator RUNX3 is transcriptionally upregulated by the NF-κB signaling pathway in KSHV-infected SLK cells and B cells during KSHV reactivation. Notably, knockdown of RUNX3 significantly promotes viral lytic replication as well as the gene transcription of KSHV. Consistent with this finding, overexpression of RUNX3 impairs viral lytic replication. Mechanistically, RUNX3 binds to the KSHV genome and limits viral replication through transcriptional repression, which is related to its DNA- and ATP-binding ability. However, KSHV has also evolved corresponding strategies to antagonize this inhibition by using the viral protein RTA to target RUNX3 for ubiquitination and proteasomal degradation. Altogether, our study suggests that RUNX3, a novel host-restriction factor of KSHV that represses the transcription of viral genes, may serve as a potential target to restrict KSHV transmission and disease development.

IMPORTANCE The reactivation of Kaposi's sarcoma-associated herpesvirus (KSHV) from latent infection to lytic replication is important for persistent viral infection and tumorigenicity. However, reactivation is a complex event, and the regulatory mechanisms of this process are not fully elucidated. Our study revealed that the host RUNX3 is upregulated by the NF-κB signaling pathway during KSHV reactivation, which can repress the transcription of KSHV genes. At the late stage of lytic replication, KSHV utilizes a mechanism involving RTA to degrade RUNX3, thus evading host inhibition. This finding helps elucidate the regulatory mechanism of the KSHV life cycle and may provide new clues for the development of therapeutic strategies for KSHV-associated diseases.

KEYWORDS KSHV, RUNX3, transcriptional regulation, RTA

Kaposi's sarcoma-associated herpesvirus (KSHV), also known as human herpesvirus 8, is a human oncogenic gamma herpesvirus that can cause Kaposi's sarcoma, primary effusion lymphoma, and multicentric Castleman disease (1–3). Similar to other herpesviruses, the life cycle of KSHV can be separated into two phases: latent infection and lytic replication (4). During the initial infection, KSHV establishes a latency for lifelong persistent infection to evade host immune surveillance. Only a few infectious viral progenies are produced during this period. Multiple copies of the viral genome are tethered to cellular chromosomes by KSHV latency-associated nuclear antigen (LANA) in the form of circular episomes (5, 6). KSHV gene expression is highly restricted, except a few genes, such as ORF71 (vFLIP), ORF72 (vCyclin), ORF73 (LANA), kaposins, and 25

Editor Jae U. Jung, Lerner Research Institute, Cleveland Clinic, Cleveland, Ohio, USA

Address correspondence to Ke Lan, klan@whu.edu.cn.

Pengyu Ren and Danping Niu contributed equally to this article. Author order was determined in order of increasing seniority.

The authors declare no conflict of interest.

Received 7 October 2023
Accepted 11 December 2023
Published 10 January 2024

mature microRNAs (7). These gene products play important roles in regulating the transcription of latent viral genes, inhibiting viral lytic gene expression, maintaining viral episomes, evading host immune surveillance, and promoting cell proliferation (8–11). Although the default life cycle of KSHV is latent infection, both spontaneous reactivation and induced reactivation of the viral genome occur, causing all viral genes to be expressed in large quantities and producing infectious viral particles. These events are critical for KSHV-mediated tumorigenesis and cancer development (12–14). Therefore, exploring the molecular events in the cell as well as the virus during the phase of KSHV lytic replication is essential to fully understand the pathogenesis of KSHV.

KSHV enters the lytic replication phase in response to numerous environmental factors or pathophysiological stimuli, such as hypoxia, oxidative stress, viral coinfection, and induction by chemical agents (15). During viral reactivation, the replication and transcription activator (RTA) encoded by KSHV ORF50 plays a decisive role. Overexpression of RTA is sufficient to disrupt KSHV latency and promote viral lytic replication (16). RTA is a functionally diverse protein. In addition to functioning as a transcriptional regulator, it can act as an E3 ubiquitin ligase to target host or viral proteins for proteasomal degradation. Examples include IRF3, IRF7, MyD88, and NF-κB, which are associated with natural immunity, repressors such as SMC5/6 and K-RBP, and the viral proteins LANA and vFLIP (17–22). Many proteins that are targeted for degradation by RTA have not been identified. The exploration of these proteins is important for elucidating the molecular mechanisms of the KSHV life cycle.

In mammals, there are three members of the Runt-related (RUNX) family: RUNX1, RUNX2, and RUNX3. They have a highly conserved "Runt" structural domain, which is a DNA-binding and heterodimerization region of approximately 120 amino acids that regulate transcription by binding to the core binding factor β (CBFβ) (23–25). RUNX genes show tissue-specific differential expression and often play important roles in regulating development and differentiation. RUNX1 (also known as AML-1) has an important role in hematopoiesis and its dysfunction leads to leukemia (26). RUNX2 (also known as AML-3) has a critical function in the process of osteogenesis (27). Moreover, RUNX3 (also known as AML-2) is involved in various signaling pathways, such as the TGF-β pathway and the Wnt signaling pathway, and regulates their functions, affecting cell proliferation, apoptosis, angiogenesis, cell adhesion, and tumor invasion (28). Therefore, RUNX3 is strongly associated with the development of a variety of cancers. There is evidence that mutations in RUNX family proteins are often found in common human diseases. For example, RUNX1 mutations are often found in leukemia and breast cancer (29, 30). Mutation of RUNX3 often occurs in gastric cancer (31). However, whether these disease-associated mutations in RUNX family proteins affect their ability to regulate viruses has not been explored.

In recent years, increasing evidence has shown that RUNX family proteins can be involved in the viral life cycle and pathogenesis of viral infections. For instance, RUNX1 promotes influenza A virus (IAV) by inhibiting type I interferon signaling, while RUNX3 inhibits IAV by promoting apoptosis (32, 33). In addition, RUNX1 can directly bind to the herpes simplex virus type I (HSV-1) genome to inhibit viral gene expression and lytic infection (34). Epstein-Barr virus (EBV) can drive RUNX3 to repress RUNX1 transcription, which is essential for EBV-mediated immortalized B-cell proliferation (35). These studies suggest that the proteins of the RUNX family play important roles in viruses with either positive or negative functions. However, the roles of the RUNX family in KSHV infection have yet to be defined.

In the present study, we found that RUNX3 is transcriptionally upregulated during the reactivation of KSHV and that this upregulation is mediated by the NF-κB signaling pathway. Remarkably, knockdown of RUNX3 significantly enhances KSHV lytic replication, whereas overexpression of RUNX3 hinders viral lytic replication. Further studies showed that RUNX3 can directly bind to the genome of KSHV and function as a transcriptional repressor. This regulatory function is related to the DNA- and ATP-binding activity of RUNX3. However, KSHV RTA can degrade RUNX3. Our study demonstrated that

RUNX3, as a novel host restriction factor targeting KSHV, can restrain KSHV lytic gene expression and lytic replication.

RESULTS

RUNX3 expression is upregulated by NF-κB during KSHV lytic reactivation

Previous studies have shown that RUNX family proteins, a family of transcriptional regulators, are involved in the life cycle of multiple herpesviruses and play various roles in different herpesviruses (34, 36). This implies that RUNX family plays important roles in herpesviral infections. However, the functional role of RUNX proteins in KSHV is unknown. To investigate whether the RUNX family is involved in the life cycle of KSHV, especially in the lytic reactivation phase, which is highly correlated with viral transcription, we first examined the kinetics of RUNX1, RUNX2, and RUNX3 expression in KSHV-positive iSLK.RGB cells during KSHV lytic reactivation. The iSLK.RGB cell line was stably infected by a recombinant reporter virus called red-green-blue-BAC16 (RGB-BAC16), which can be used to visualize the life cycle of KSHV by fluorescence, with red fluorescence indicating infected cells and green fluorescence indicating KSHV lytic replication (37). After iSLK.RGB cells were induced by doxycycline (Dox), which is an inducer of KSHV lytic replication (38), KSHV entered a period of lytic reactivation. Both protein and mRNA expression of RUNX3 were significantly upregulated during this period (Fig. 1C and D). Interestingly, we observed a decrease in RUNX3 protein levels after 72 h of lytic reactivation compared to 48 h. However, the changes in RUNX1 and RUNX2 were not as significant as those in RUNX3 (Fig. 1A, B and D). Therefore, we focused our research on RUNX3. To verify the reliability of this phenomenon, we repeated this experiment in KSHV-positive BCBL1 cells. After BCBL1 cells were treated with 12-*O*-tetradecanoylphorbol-13-acetate (TPA) and sodium butyrate (NaB), which are also inducers of KSHV lytic replication (39), we obtained the same results as those observed in iSLK.RGB cells (Fig. 1E and F).

Previously, it has been shown that RUNX3 expression can be induced by interferon and NF-κB signaling pathways (33, 40). Therefore, we treated iSLK.RGB cells with the IFN inhibitor BX795 and the NF-κB inhibitor BAY-7082, respectively. Interestingly, we found that interferon inhibitors had almost no effect on the upregulation of RUNX3 (Fig. S1A and B), while NF-κB inhibitors almost completely blocked the upregulation of RUNX3 (Fig. 1G and H). Moreover, we transfected two separate siRNAs targeting human NF-κB p65 into iSLK.RGB cells to reduce p65 expression levels before Dox induction. The designed siRNA was able to significantly reduce the mRNA and protein levels of p65 (Fig. 1I and J). Moreover, the expression of RUNX3 during KSHV lytic reactivation was also downregulated by knocking down p65 (Fig. 1I and J). These results confirm that the NF-κB signaling pathway plays an important role in the upregulation of RUNX3 during KSHV lytic reactivation.

Knockdown of RUNX3 promotes the replication process of KSHV

To explore the role of RUNX3 in KSHV lytic replication, two separate siRNAs targeting human RUNX3 were transfected into iSLK.RGB cells to reduce RUNX3 expression levels before Dox induction. The siRNAs reduced the expression level of RUNX3 by ~40% (Fig. 2A and B). The iSLK.RGB cells that were pretransfected with nonspecific (NS) siRNAs and RUNX3 siRNAs were treated with Dox for 48 and 72 h to induce KSHV lytic replication. Knockdown of RUNX3 increased the proportion of GFP-positive iSLK.RGB cells (Fig. 2C). We next monitored KSHV virus particles in the supernatant and in iSLK.RGB cells. Consistent with GFP expression levels, knockdown of endogenous RUNX3 expression significantly increased KSHV replication (Fig. 2D) and KSHV virus particle production (Fig. 2E). Moreover, the transcript levels of viral genes were increased after knocking down RUNX3 (Fig. 2G). In addition, HEK293T cells were infected with viral progeny particles in an equal volume of cell culture supernatant, and GFP fluorescence intensity was significantly enhanced in the two RUNX3 knockdown groups compared to the control group (Fig. 2F).

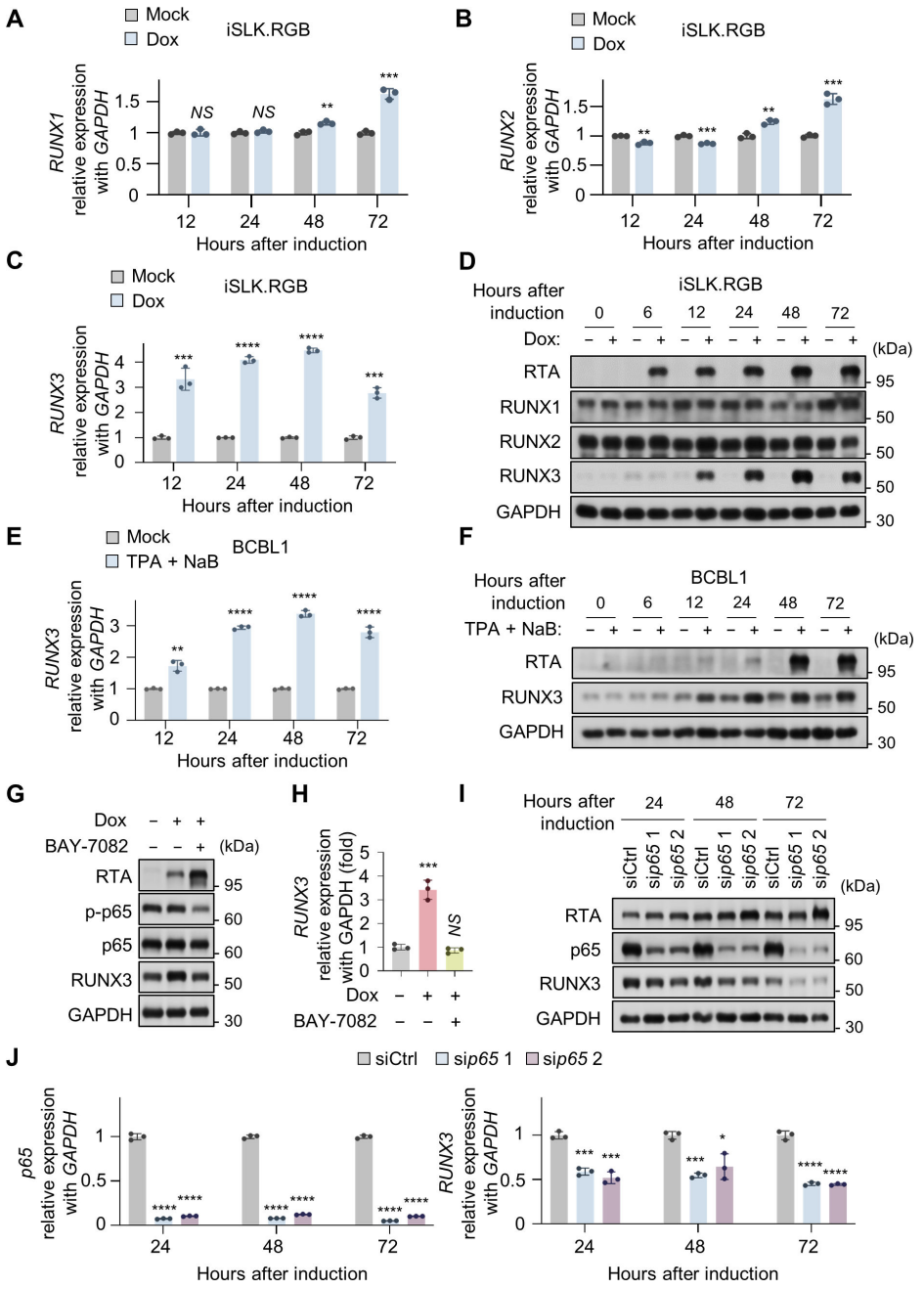

FIG 1 RUNX3 expression is upregulated by NF-κB during KSHV lytic reactivation. (A–D) iSLK.RGB cells were treated with or without doxycycline (Dox). The kinetics of RUNX family expression in iSLK.RGB cells. (A) The mRNA of RUNX1 during the induction of lytic reactivation in iSLK.RGB cells were analyzed by qPCR. (B) The mRNA of RUNX2 during the induction of lytic reactivation in iSLK.RGB cells were analyzed by qPCR. (C) The mRNA of RUNX3 during the induction of lytic reactivation in iSLK.RGB cells were analyzed by qPCR. (D) iSLK.RGB cells were induced with Dox for indicated times. The expression levels of RTA and RUNX family were examined by western blotting. (E and F) BCBL1 cells were treated with or without 12-*O*-tetradecanoylphorbol-13-acetate (TPA) and sodium butyrate (NaB). The kinetics of RUNX3 expression in BCBL1 cells. (E) BCBL1 cells were induced with TPA and NaB for indicated times. The mRNA of RUNX3 during the induction of lytic reactivation in BCBL1 cells were analyzed by qPCR. (F) The expression levels of RTA and RUNX3 were examined by western blotting. (G–J) RUNX3 induction is mediated primarily by NF-κB pathways during KSHV lytic reactivation. (G) iSLK.RGB cells were treated with or without 10 μM BAY11-7082 for 6 h in advance and then treated with or without Dox for 24 h. The expression of RUNX3 was detected by western blots. (H) The mRNA expression of RUNX3 was determined by qPCR analysis. iSLK.RGB cells were transfected with control siRNA and two siRNAs specific to human NF-κB p65. Twenty-four hours after

(Continued on next page)

FIG 1 (Continued)

transfection, cells were treated with Dox for the indicated times. The knockdown efficiency and RUNX3 expression were determined by western blots (I) and qPCR (J). Data were shown as mean ± SD (error bars) from at least three independent experiments, and statistical analysis was done by using multiple unpaired student's *t* test (A, B, C, E, and J) and unpaired student's *t* test (H). ns, not significant; **P* < 0.05; ***P* < 0.01; ****P* < 0.001; *****P* < 0.0001.

Ectopic expression of RUNX3 suppresses the lytic replication of KSHV

To further confirm the effect of RUNX3 on KSHV lytic replication, iSLK.RGB cells were transduced with a lentivirus containing Flag-tagged RUNX3 (iSLK.RGB-RUNX3) or a control lentivirus (iSLK.RGB-Vector). RUNX3 expression in iSLK.RGB-RUNX3 cells was determined by qPCR (Fig. 3C) and an anti-Flag antibody (Fig. 3A and B) or anti-RUNX3 antibody (Fig. S1C). After 48 and 72 h of Dox-induced RTA expression, we found that there were significantly fewer GFP-positive cells in the iSLK.RGB-RUNX3 group compared to the control group (Fig. 3D). Similarly, overexpression of RUNX3 significantly inhibited replication of the KSHV genome (Fig. 3E) and the production of KSHV viral particles (Fig. 3F). As shown in Fig. 3G, the transcript levels of both lytic and latent KSHV genes were reduced in RUNX3 stable expression cell lines. This result is in line with the fact that the protein expression of RTA was also downregulated by the overexpression of RUNX3 (Fig. 3B). In addition, to further confirm the effect of RUNX3 on the infectivity of viral progeny, we used viral progeny particles in an equal volume of cell supernatant to infect HEK293T cells. The results showed that HEK293T cells infected with the supernatants from the iSLK.RGB-RUNX3 cell group had a lower green fluorescent signal (Fig. 3H). In conclusion, these results strongly suggest that RUNX3 can effectively inhibit the replication of KSHV.

RUNX3 binds to the promoter of the KSHV gene and represses its transcription

RUNX3 can act as a transcription factor that directly binds to the promoter of genes to regulate their expression (36, 41, 42). Our results suggest that RUNX3 has an inhibitory effect on the transcription of KSHV genes (Fig. 2G and 3G). Therefore, to determine whether RUNX3 represses KSHV gene transcription through transcriptional regulation, we first performed a dual luciferase reporter gene assay. The results showed that RUNX3 inhibited RTA-mediated activation of ORF57, ORF59, PAN, and K8.1 promoters in a dose-dependent manner (Fig. 4A through D). To determine whether RUNX3 binds to the KSHV genome, we performed a chromatin immunoprecipitation (ChIP) assay. ChIP experiments were performed in iSLK.RGB and BCBL1 cells using an anti-RUNX3 antibody or IgG antibody and primers targeting the promoter regions of representative genes from different periods of the KSHV life cycle. We observed that in iSLK.RGB (Fig. 4E) and BCBL1 (Fig. 4F) cell lines, the RUNX3 antibody coprecipitated the promoters of KSHV genes at different stages with varied efficiencies. To verify the reliability of this result, we further used BrdU to tag the newly synthesized KSHV genome (43). To ensure that BrdU was only incorporated into the KSHV genome, cells were fixed and stained with BrdU antibody and RUNX3 antibody after 2 h of BrdU labeling. In BCBL1 cells, RUNX3 was mainly localized in the nucleus. In the absence of TPA treatment, KSHV underwent little lytic replication and, therefore, BrdU could not be detected. However, BrdU-labeled viral DNA could be observed in TPA and NaB-treated BCBL1 cells and was mostly colocalized with RUNX3 in the nucleus (Fig. 4G).

Transcriptional repression of KSHV by RUNX3 is related to its DNA- and ATP-binding ability

The above results indicate that RUNX3 can bind to KSHV genomic DNA to inhibit gene transcription. To further explore the molecular mechanism by which RUNX3 represses KSHV transcriptional replication, we constructed a series of common mutations in different malignant tumors as follows: R122C, R143Q, G145E, T151A, and the R143Q&G145E double mutant (DM) (Fig. 5A). R122 is frequently found in RUNX3 in

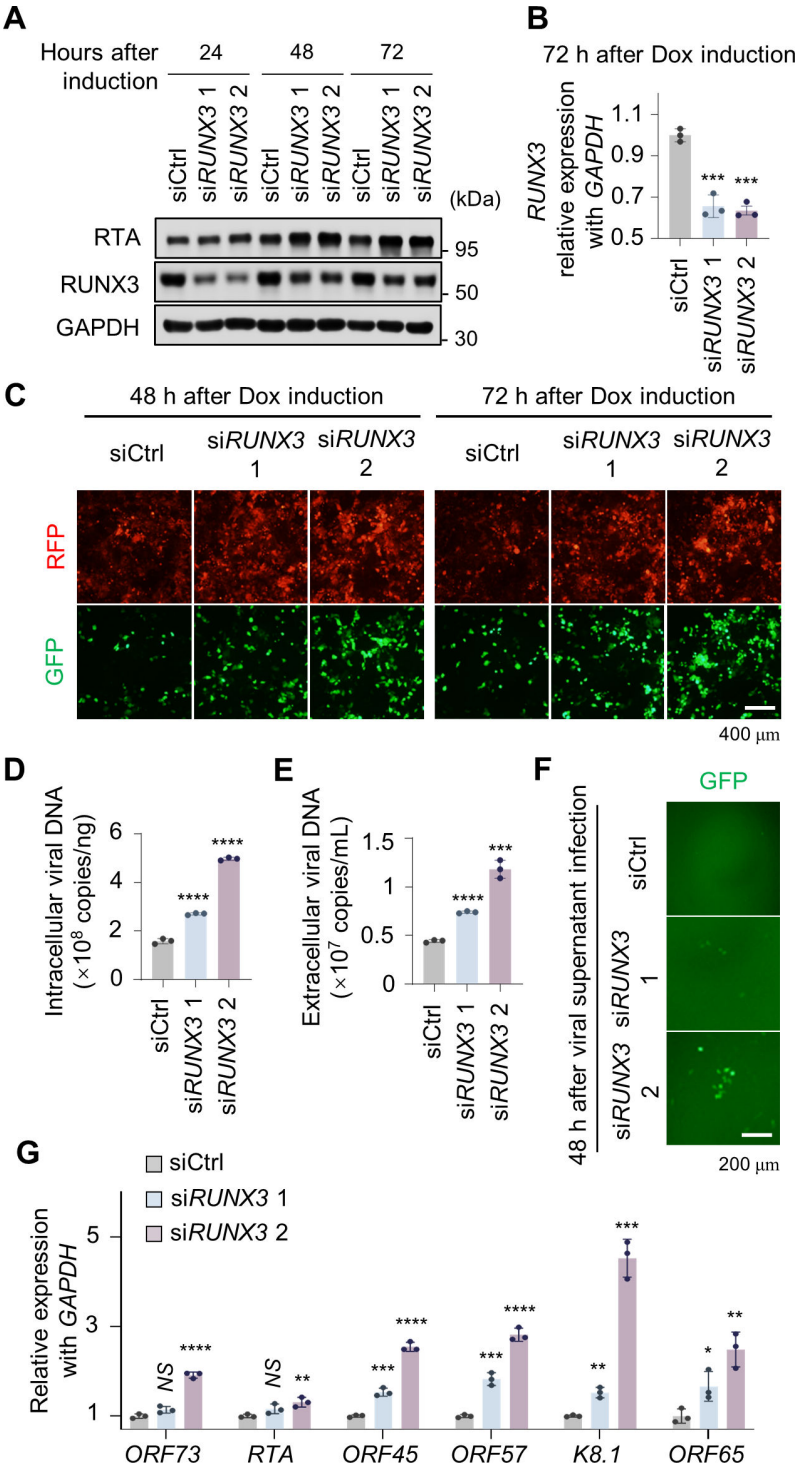

FIG 2 Knockdown of RUNX3 promotes the replication process of KSHV. iSLK.RGB cells were transfected with control siRNA and two siRNAs specific to human RUNX3. Twenty-four hours after transfection, cells were treated with Dox for the indicated times. The knockdown efficiency was determined by western blots (A) and qPCR (B). (C) GFP-positive (Lytic) cells were observed by fluorescence microscope. (D and E) Intracellular KSHV genomic DNA and extracellular KSHV DNA were extracted from Dox-induced iSLK.RGB cells or cell supernatants. Copy numbers of KSHV genomic DNA were determined using the qPCR method with the K9 primer. (F) HEK293T cells were infected with supernatants from RUNX3-knockdown cells for 48 h. Then, KSHV-infected GFP-positive cells were observed by fluorescence microscope.
(Continued on next page)

FIG 2 (Continued)

(G) The transcriptional levels of the KSHV gene were analyzed by qPCR at 48 h after Dox induction. Data were shown as mean ± SD (error bars) from at least three independent experiments, and statistical analysis was done by using multiple unpaired student's *t* test (G) and unpaired student's *t* test (B, D, and E). ns, not significant; *$P < 0.05$; **$P < 0.01$; ***$P < 0.001$; ****$P < 0.0001$.

gastric cancer, and mutations at this site are thought to affect the DNA-binding ability of the Runt structural domain (31). In breast cancer, the RUNX1 equivalents of R143 and G145 are mutated. Moreover, mutations in R143 and G145 are thought to affect ATP binding in the Runt structural domain (30). In addition, T151 is a putative site of phosphorylation by AKT kinase (44). This phosphorylation affects the transcriptional activity

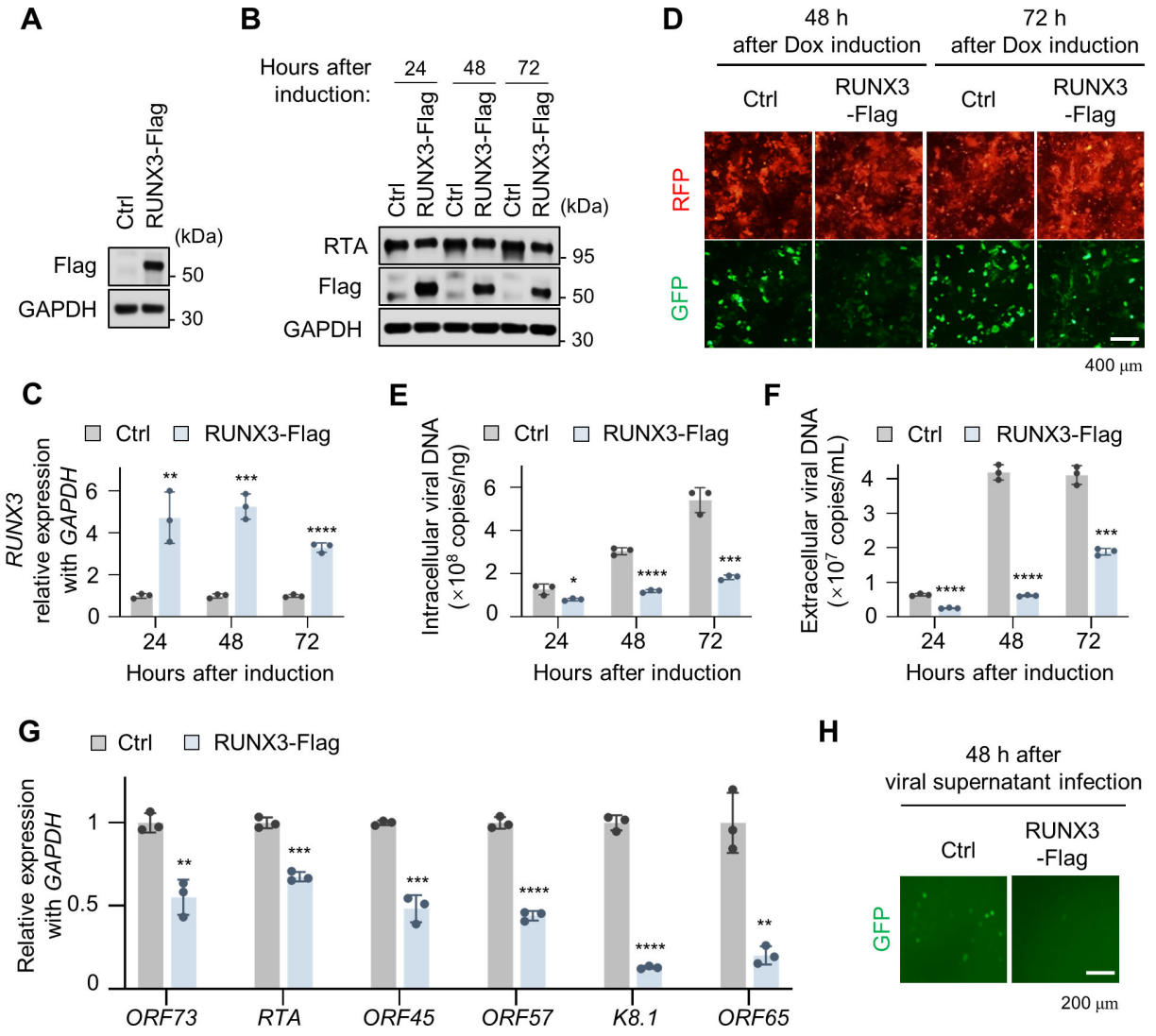

FIG 3 Ectopic expression of RUNX3 suppresses the lytic replication of KSHV. iSLK.RGB cells were stably transduced with lentivirus containing RUNX3-Flag expression plasmids or Vector-Flag plasmids. The expression of RUNX3 was evaluated by western blotting (A and B) and qPCR (C). (D) GFP-positive (Lytic) cells were observed by fluorescence microscope. (E and F) Intracellular KSHV genomic DNA and extracellular KSHV DNA were extracted from Dox-induced iSLK.RGB cells or cell supernatants. Copy numbers of KSHV genomic DNA were determined using the qPCR method with the K9 primer. (G) The transcriptional levels of the KSHV gene were analyzed by qPCR at 48 h after Dox induction. (H) HEK293T cells were infected with supernatants from RUNX3-overexpressing cells for 48 h. Then, KSHV-infected GFP-positive cells were observed by fluorescence microscope. Data were shown as mean ± SD (error bars) from at least three independent experiments, and statistical analysis was done by using Multiple unpaired student's *t* test (C, E, F, and G). ns, not significant; *$P < 0.05$; **$P < 0.01$; ***$P < 0.001$; ****$P < 0.0001$.

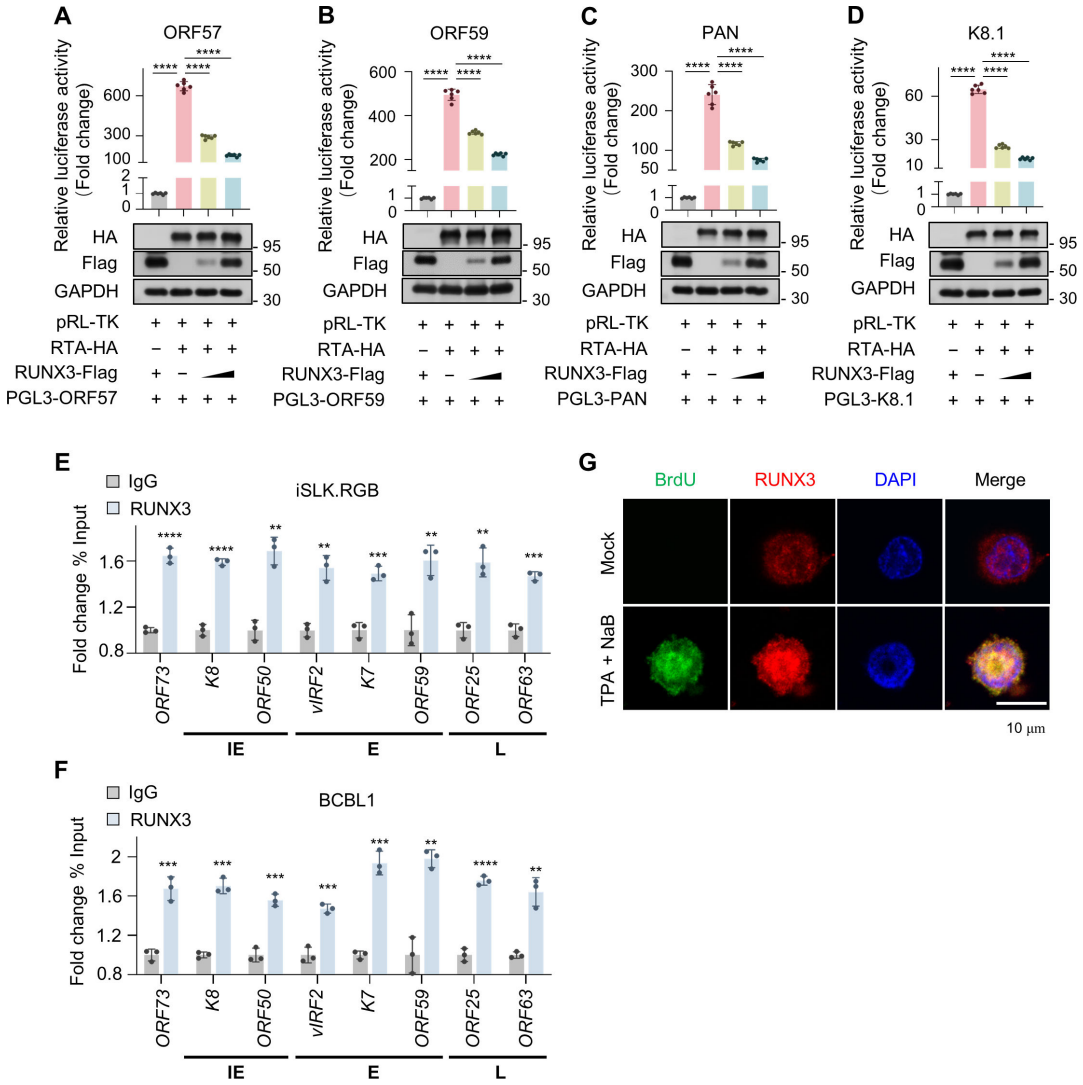

FIG 4 RUNX3 binds to the promoter of the KSHV gene and represses its transcription. (A–D) Effect of RUNX3 on RTA-mediated activation of ORF57, ORF59, PAN, and K8.1 promoters. HEK293T cells were transfected with the indicated plasmids for 36 h. The cells were then lysed by cell lysis buffer and assayed for luciferase activity. For these experiments, values are normalized to values for the Renilla luciferase control. (E and F) ChIP analysis of RUNX3 in iSLK.RGB and BCBL1 cells. RUNX3 was immunoprecipitated from isolated nuclei of iSLK.RGB and BCBL1 cells and bound DNA was analyzed by CHIP-qPCR assay with primers specific to regions (~100 to 200 bp) flanking the transcription start sites of the indicated genes. Data were calculated as the fold change in percentage of input DNA compared with control ChIP experiment. (G) Colocalization of RUNX3 with KSHV genomic DNA. BCBL1 cells were treated with TPA (20 ng/mL) and NaB (1 mM) for 24 h and then incubated with BrdU for 2 h, followed by immunofluorescence to observe colocalization of endogenous RUNX3 and KSHV genomic DNA. Data were shown as mean ± SD (error bars) from at least three independent experiments, and statistical analysis was done by using multiple unpaired student's *t* test (E and F) and unpaired student's *t* test (A, B, C, and D). ns, not significant; **P* < 0.05; ***P* < 0.01; ****P* < 0.001; *****P* < 0.0001.

of RUNX3 (45). To compare the transcriptional repressor activity of wild-type RUNX3 and mutant RUNX3, we cotransfected wild-type or mutant RUNX3 with the promoters of ORF57, ORF59, PAN, and K8.1 and repeated the previous dual-luciferase reporter gene assay. The results showed that mutations at the sites R122C, R143Q, G145E, and R143Q&G145E abrogated its transcriptional inhibitory activity, whereas the T151A mutation does not result in a significant change (Fig. 5B through E).

It has been reported that R122C, a unique mutation in RUNX3, directly affects the activity of RUNX3, resulting in the loss of its tumor suppressor function (31). We wanted

to further explore whether this mutation could similarly affect its viral suppression function in cells, so we constructed an iSLK.RGB cell line with R122C overexpression (iSLK.RGB-R122C) (Fig. 6A). Expression of the R122C mutant in iSLK.RGB-R122C cells was verified by qPCR (Fig. 6C) and an anti-Flag antibody (Fig. 6B) or an anti-RUNX3 antibody (Fig. S1D). After 48 and 72 h of Dox-induced RTA expression, we found that the proportion of GFP-positive cells in the iSLK.RGB-R122C group was essentially equal to that of the control group and significantly higher than that of the RUNX3 group (Fig. 6F). The replication of the KSHV genome (Fig. 6D) and the number of KSHV virus particles produced (Fig. 6E) after overexpression of R122C were also higher than those in the RUNX3 group and even in the control group. Similarly, the transcriptional repression levels of KSHV genes at various stages in the R122C group were restored to different degrees compared to those in the RUNX3 group (Fig. 6G). In summary, we conclude that the transcriptional repression of the KSHV gene by RUNX3 is related to its DNA-binding and ATP-binding capacities.

RTA targets RUNX3 for ubiquitination and proteasomal degradation

We observed that Dox treated iSLK.RGB cells showed a decrease in the expression level of RUNX3 protein starting from 48 h post treatment, but the RNA levels were not significantly changed (Fig. 7A and B). It is possible that KSHV has a certain strategy to prevent transcriptional repression by RUNX3 during lytic reactivation. Previously, different groups have shown that KSHV RTA also has ubiquitin E3 ligase activity and can target multiple proteins for proteasome-mediated degradation (17, 19, 21, 22, 46). It is possible that KSHV utilizes a similar strategy to reduce the expression level of RUNX3 and protect the process of lytic reactivation. To test this hypothesis, we cotransfected increasing amounts of RTA expression plasmid and fixed amounts of RUNX3 expression plasmid into HEK293T cells. The results showed that RTA downregulated the protein expression of RUNX3 in a dose-dependent manner (Fig. 7C) but did not affect the mRNA expression of RUNX3 (Fig. 7D). To confirm this phenomenon, we further analyzed the changes of RUNX3 expression in iSLK.Puro cells and obtained the same results (Fig. 7E and F). The iSLK.Puro cells were selected by transferring the tetracycline-induced exogenous RTA expression system into SLK cell lines screened with hygromycin B. iSLK.Puro cells can be induced by Dox to produce RTA proteins but do not contain the KSHV viral genome. In addition, HEK293T cells were transfected with or without RTA-expressing plasmids. Then, the cells were treated with cycloheximide (CHX) 24 h after transfection. We found that RTA significantly decreased the half-life of RUNX3 (Fig. 7G and H). To further explore whether RTA degrades the RUNX3 complex via the proteasome pathway, we treated cells with the proteasome inhibitor MG132. As shown in Fig. 7I, the expression level of RUNX3 decreased due to the presence of RTA. However, the expression level of RUNX3 was significantly restored with MG132 treatment. Finally, we also assessed the effect of RTA on RUNX3 ubiquitination. The results showed that coexpression of RTA with RUNX3 caused a significant increase in the ubiquitination level of RUNX3 compared to that of the control (Fig. 7J). Altogether, these results suggest that RTA targets RUNX3 for ubiquitination and proteasomal degradation.

RTA interacts with RUNX3

To determine whether the degradation of RUNX3 by RTA occurs through direct protein-protein interactions, we first performed coimmunoprecipitation experiments in HEK293T cells. HEK293T cells were transfected with RUNX3-Flag and RTA-HA expression plasmids separately or together. Forty-eight hours post transfection, cell lysates were immunoprecipitated with anti-Flag antibody. The results showed that RTA could be successfully immunoprecipitated by RUNX3 (Fig. 8A). Similarly, the reverse coimmunoprecipitation assay showed an association between RTA and RUNX3 (Fig. 8B). To further confirm if whether endogenous RUNX3 also interacts with RTA, we performed a coimmunoprecipitation assay using iSLK.RGB and BCBL1 cells. After treating iSLK.RGB and BCBL1 cells

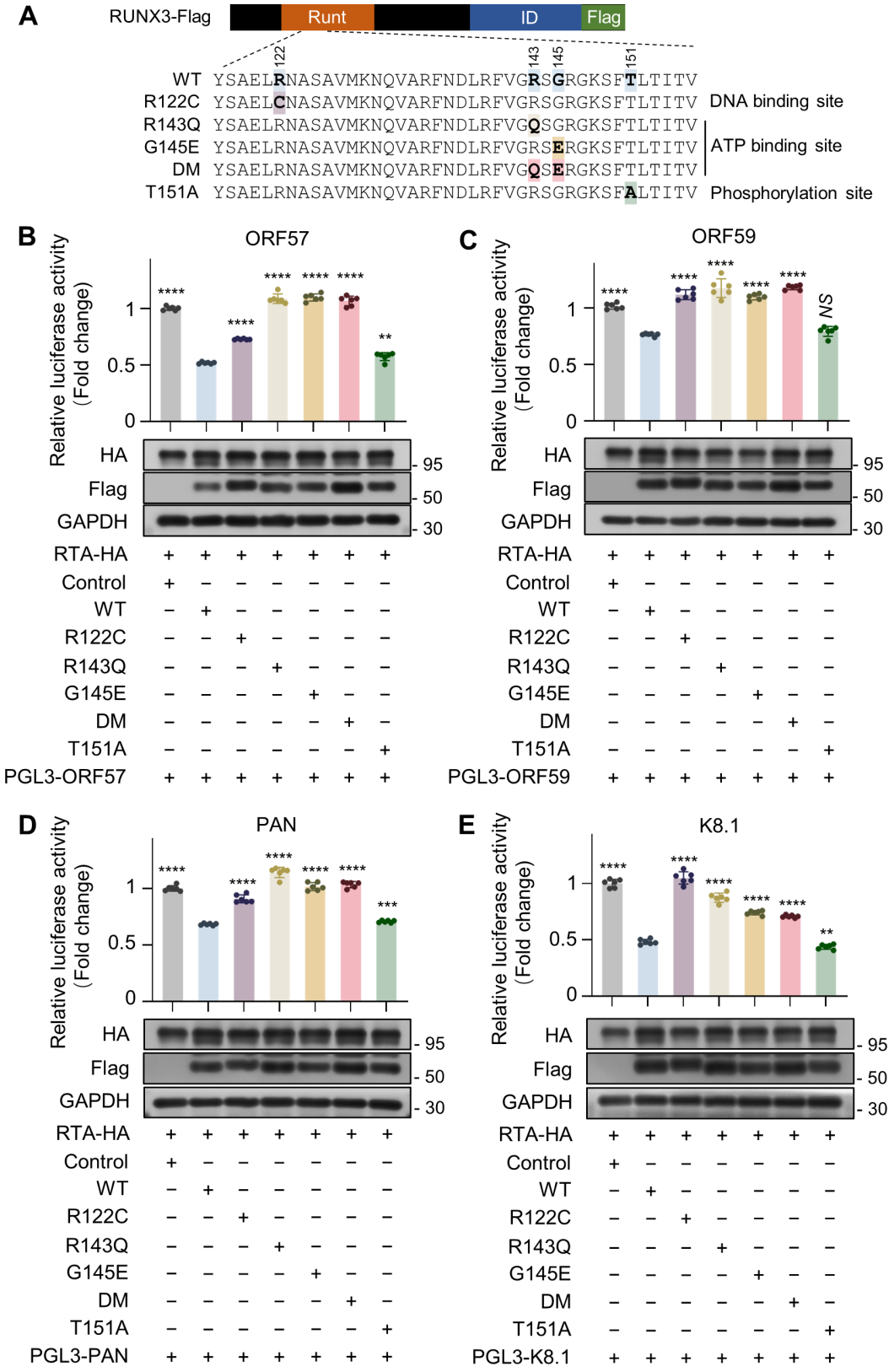

FIG 5 Transcriptional repression of KSHV by RUNX3 is related to its DNA- and ATP-binding ability. (A) Schematic representation of DNA binding, ATP binding and phosphorylation site mutations within the Runt structural domain of RUNX3. Black background represents the entire RUNX3, orange represents the "Runt" DNA binding domain, blue represents the "ID"

(Continued on next page)

FIG 5 (Continued)

inhibitory domain, and green represents the Flag Tag. (B–E) Effect of R122C, R143Q, G145E, R143Q&G145E (DM), T151A on RTA-mediated activation of ORF57, ORF59, PAN, and K8.1 promoters. HEK293T cells were transfected with the indicated plasmids for 36 h. The cells were then lysed by cell lysis buffer and assayed for luciferase activity. For these experiments, values are normalized to values for the Renilla luciferase control. Data were shown as mean ± SD (error bars) from at least three independent experiments, and statistical analysis was done by using unpaired student's *t* test (B, C, D, and E). ns, not significant; **P* < 0.05; ***P* < 0.01; ****P* < 0.001; *****P* < 0.0001.

with inducers for 48 h, cell lysates were collected and immunoprecipitated with anti-RTA antibody or IgG control. Indeed, endogenous RUNX3 also interacts with RTA in iSLK.RGB (Fig. 8C) and BCBL1 cells (Fig. 8D) during KSHV lytic reactivation. In addition, we mapped

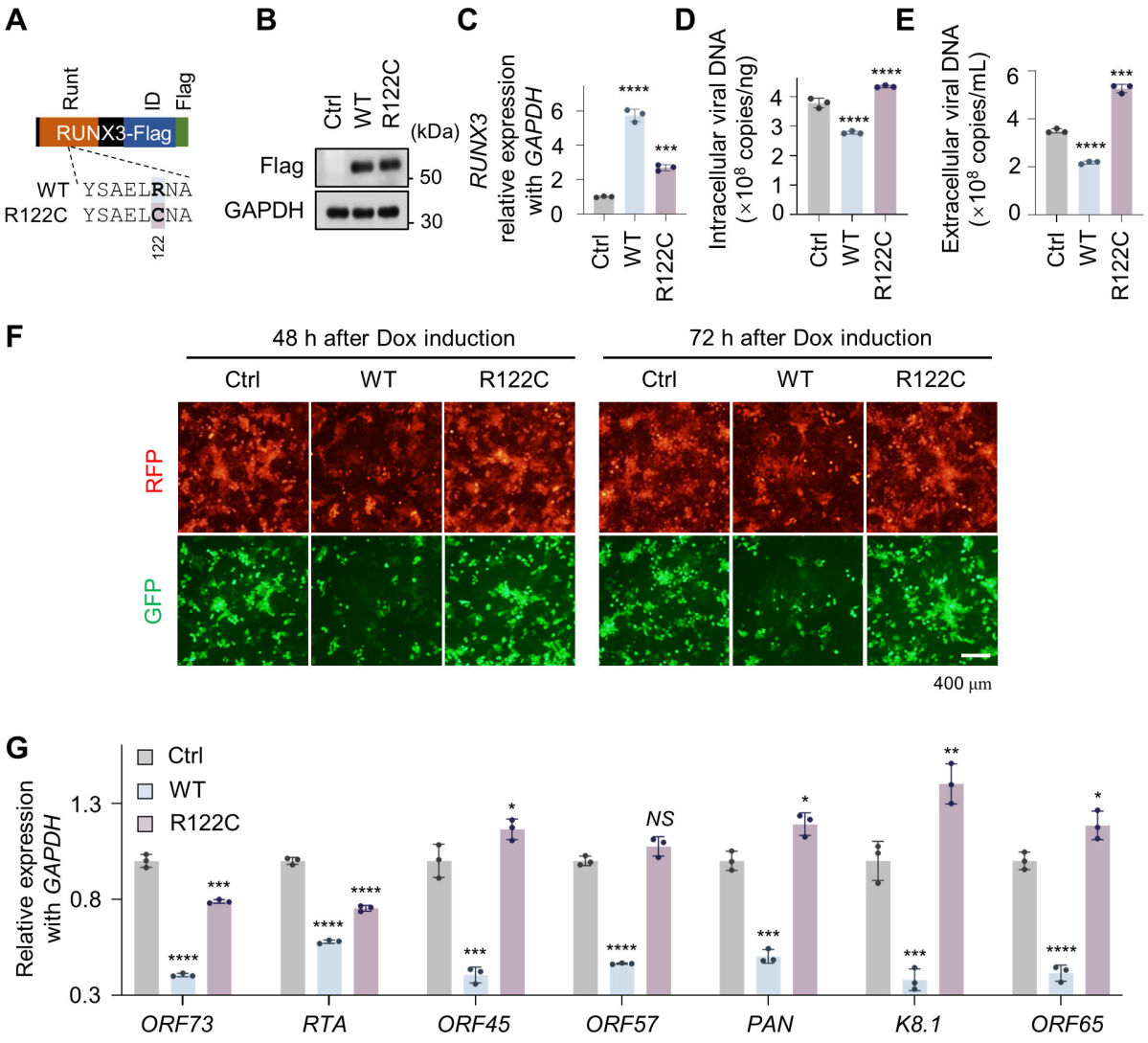

FIG 6 Ectopic expression of RUNX3-R122C does not inhibit KSHV lytic replication. (A) Schematic diagram of the RUNX3-R122C mutant. Black background represents the entire RUNX3, orange represents the "Runt" DNA-binding domain, blue represents the "ID" inhibitory domain, and green represents the Flag Tag. iSLK.RGB cells were stably transduced with lentivirus containing RUNX3-Flag expression plasmids, R122C-Flag or Vector-Flag plasmids. The expression of RUNX3 was evaluated by western blotting (B) and qPCR (C). (D and E) Intracellular KSHV genomic DNA and extracellular KSHV DNA were extracted from Dox-induced iSLK.RGB cells or cell supernatants. Copy numbers of KSHV genomic DNA were determined using the qPCR method with the K9 primer. (F) GFP-positive (Lytic) cells were observed by fluorescence microscope. (G) The transcriptional levels of the KSHV gene were analyzed by qPCR at 48 h after Dox induction. Data were shown as mean ± SD (error bars) from at least three independent experiments, and statistical analysis was done by using multiple unpaired student's *t* test (G) and unpaired student's *t* test (C, D, and E). ns, not significant; **P* < 0.05; ***P* < 0.01; ****P* < 0.001; *****P* < 0.0001.

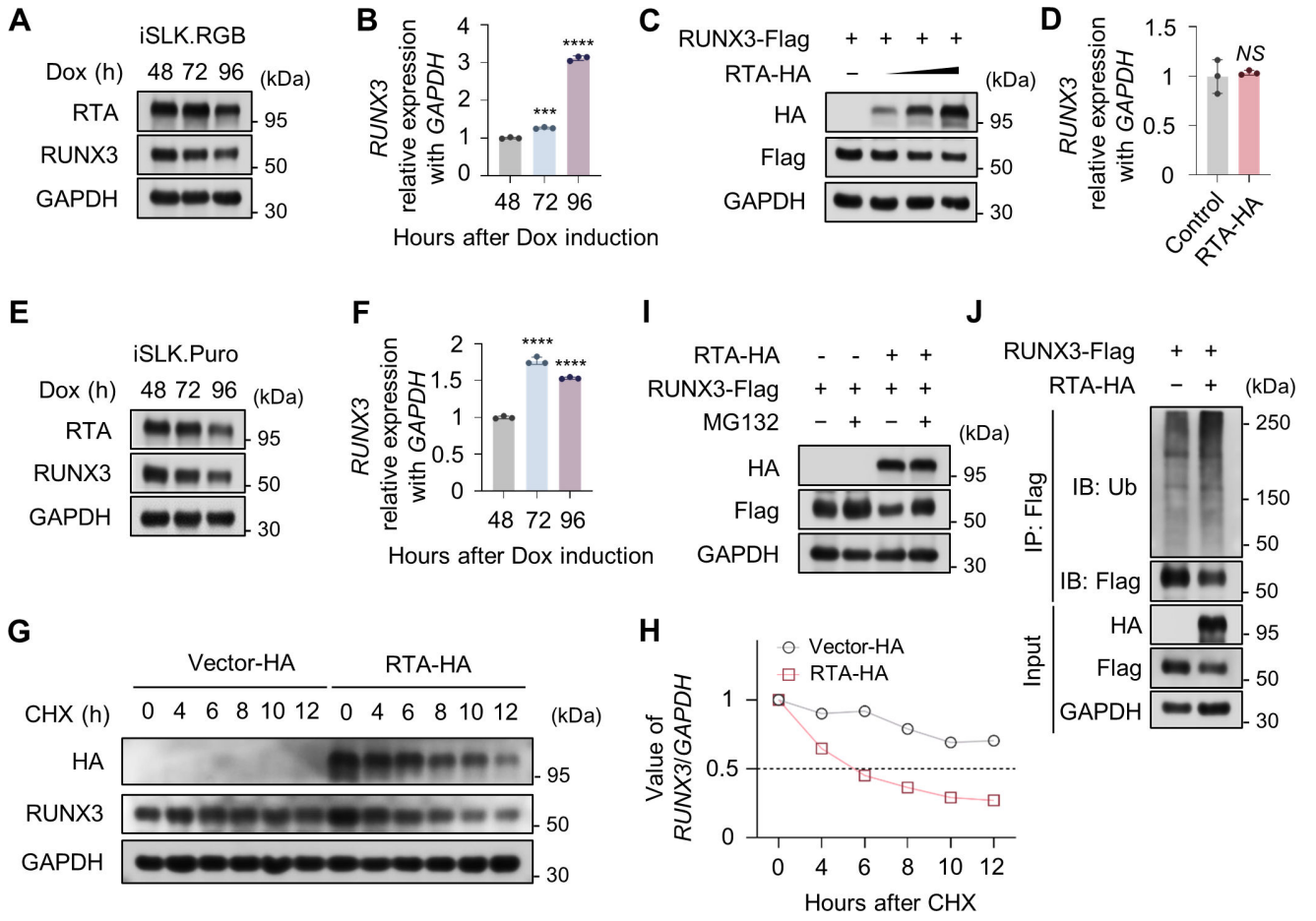

FIG 7 RTA targets RUNX3 for ubiquitination and proteasomal degradation. (A and B) The kinetics of RUNX3 expression in iSLK.RGB cells at the late stage of KSHV lysis. (A) iSLK.RGB cells were induced with Dox for indicated times. The expression levels of RTA and RUNX3 were examined by western blotting. (B) RUNX3 mRNA was analyzed by qPCR during induction of late KSHV lysis in iSLK.RGB cells. (C and D) Effect of RTA on RUNX3 expression. (C) A constant amount of RUNX3-expressing plasmid and an increasing amount of RTA-expressing plasmid were co-transfected into HEK293T cells for 48 h. The protein expression of RTA and RUNX3 was detected by western blotting. (D) HEK293T cells were transfected with or without RTA expression plasmid for 48 h, and the mRNA of endogenous RUNX3 was detected by qPCR. (E and F) The kinetics of RUNX3 expression in iSLK.Puro cells. (E) iSLK.Puro cells were induced with Dox for indicated times. The expression levels of RTA and RUNX3 were examined by western blotting. (F) The mRNA of RUNX3 was analyzed by qPCR during the induction of RTA mass expression in iSLK.Puro cells. (G and H) RTA reduces the stability of RUNX3. (G) HEK293T cells were transfected with or without the RTA expression plasmid for 24 h and then treated with 100 µg/mL cycloheximide (CHX) for different times. The expression of RTA and endogenous RUNX3 was analyzed by western blotting. (H) Relative levels of RUNX3 in immunoblots (G) were quantified by signal intensity measurements and normalized to GAPDH levels. (I and J) RTA promotes RUNX3 ubiquitination and degradation via the proteasome pathway. (I) HEK293T cells were transfected with the indicated plasmids for 36 h. Cells were then treated with 10 µM MG132 for an additional 12 h, and RUNX3 expression was analyzed by western blotting. (J) HEK293T cells were transfected with RUNX3-expressing plasmid alone or co-transfected with RTA-expressing plasmid for 36 h; cells were continued to be treated with 10 µM MG132 for 12 h. Cell lysates were immunoprecipitated with anti-Flag antibody and analyzed by western blotting with the anti-ubiquitin antibodies. Data were shown as mean ± SD (error bars) from at least three independent experiments, and statistical analysis was done by using unpaired student's *t* test (B, D, and F). ns, not significant; **P* < 0.05; ***P* < 0.01; ****P* < 0.001; *****P* < 0.0001.

the structural domain of RTA responsible for the interaction with RUNX3, showing that the region of RTA comprising amino acid (aa) residues 1–273 is the main region for the interaction between RTA and RUNX3 (Fig. S1E and F). Similarly, to identify the structural domains required for RUNX3 to interact with RTA, we constructed a series of Flag-tagged RUNX3 truncation mutants (Fig. S1G) based on previously reported work (47). The results showed that RUNX3 (from 1 aa to 373 aa) interacts most strongly with RTA (Fig. S1H). Finally, RTA and RUNX3 were mainly localized in the nucleus. Clear colocalization of

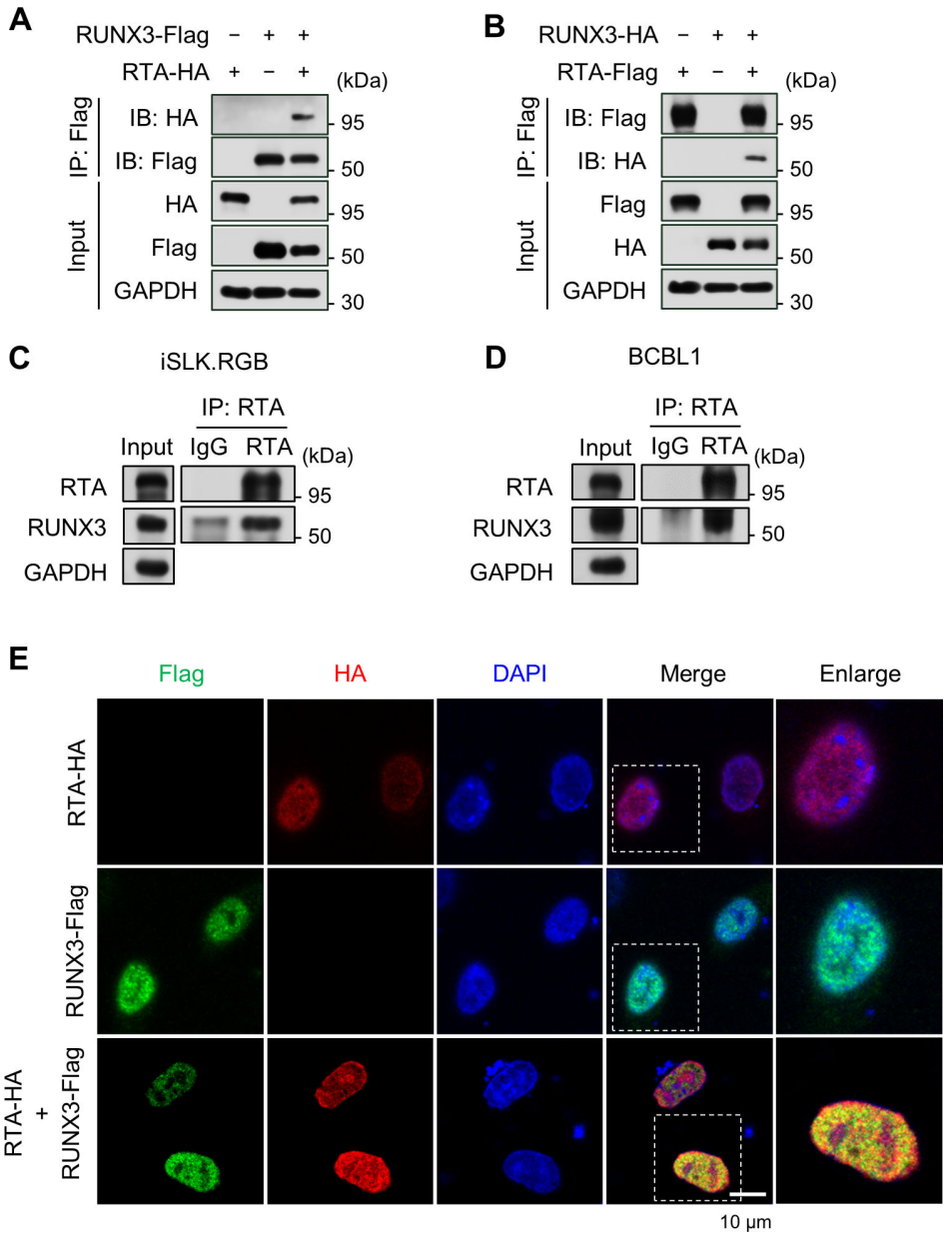

FIG 8 RTA interacts with RUNX3. (A) HEK293T cells were transfected with RTA-HA alone or RUNX3-Flag alone or RTA-HA together with RUNX3-Flag. Forty-eight hours after transfection, cell lysates were immunoprecipitated with anti-Flag antibody and analyzed by western blotting with the indicated antibodies. (B) HEK293T cells were transfected with RUNX3-HA alone or RTA-Flag alone or RUNX3-HA together with RTA-Flag. Forty-eight hours after transfection, cell lysates were immunoprecipitated with anti-Flag antibody and analyzed by western blotting with the indicated antibodies. (C and D) Co-IP of endogenous RTA and RUNX3 in iSLK.RGB and BCBL1 cells. After treatment of iSLK.RGB cells with Dox and BCBL1 cells with TPA and NaB for 48 h, cell lysates were immunoprecipitated with anti-RTA antibody or IgG control and analyzed by Western blotting with the indicated antibodies. (E) Colocalization of RUNX3 and RTA in Hela cells. Hela cells were first transfected with RTA-HA alone, RUNX3-Flag alone, or RTA-HA together with RUNX3-Flag. Then, the cells were fixed and detected with anti-HA rabbit antibody and anti-Flag mouse antibody. Finally, cells were incubated with Alexa Fluor 488 (green), Alexa Fluor 555 (red), and DAPI (blue). Colocalization was viewed by a DM6000B fluorescence microscope.

RUNX3 and RTA in the nucleus was observed in the immunofluorescence experiments (Fig. 8E). Altogether, these results confirm that RTA interacts with RUNX3.

DISCUSSION

In malignant tumors caused by KSHV, the virus is predominantly latent in the cells. Although this latent infection enables it to evade host immune surveillance and maintain persistent infection, latency alone is not sufficient to sustain the onset and progression of associated diseases (48, 49). KSHV lytic reactivation is necessary for transmission of the virus within an individual and for the transmission of the virus to other individuals (12, 50, 51). KSHV lytic reactivation is a complex process that is regulated by the interactions between host factors and viral proteins as well as multiple signaling pathways (52, 53). Exploring the molecular events during KSHV lytic reactivation is important for understanding the pathogenesis of KSHV and developing ways to block persistent KSHV infection. In this study, we identified a new host factor, RUNX3, which is upregulated by the NF-κB signaling pathway during KSHV lytic reactivation and is able to inhibit the transcription of the KSHV genome, thus suppressing the production of viral particles. Our work revealed for the first time that RUNX3 is involved in the KSHV life cycle, providing novel insights into the herpesvirus lytic phase and completing the functional knowledge of RUNX3 in the area of herpesvirus.

It is known that the transcription factor RUNX3 can play a role in the development of cells in the nerves, thymus, stomach, and intestines (31, 54, 55). Only a few studies have addressed the relationship between RUNX3 and viruses. Gan et al. showed that RUNX3 was able to inhibit IAV by promoting apoptosis (33). In contrast, RUNX3 expression is necessary for the efficient proliferation of B cells immortalized by EBV (36). These studies suggest that RUNX3 plays varying functional roles in different viral infections. We used dual luciferase reporter gene assay, CHIP and BrdU insertion experiments to show that RUNX3 can bind to the genome of KSHV to repress viral gene transcription. Our results indicate that RUNX3 exhibits distinct repressive capabilities on different KSHV viral genes, suggesting the possibility of promoter-specificity for RUNX3.

The R122C mutation in RUNX3 occurs frequently in a variety of cancers and affects the DNA-binding ability of RUNX3 (31). In breast cancer, RUNX1-equivalent R143 and G145 mutations are thought to affect ATP binding (30). Dual luciferase reporter assays showed that the R122C, R143Q, and G145E mutations significantly impaired the ability of RUNX3 to inhibit the KSHV gene promoter. This finding suggests that transcriptional repression of KSHV by RUNX3 is related to its DNA- and ATP-binding ability. T151 is a RUNX3 putative ATK kinase phosphorylation site, and phosphorylation promotes sumoylation modifications that, in turn, affect the transcriptional function of RUNX3 (45). The activation of the KSHV gene promoter was not significantly changed by the T151A mutation, suggesting that this modification may not be required for RUNX3 to induce transcriptional repression of KSHV. Our work is the first to apply disease-associated mutants of RUNX3 to viral research and revealed how RUNX3 functions as a transcriptional regulator in the viral genome, which provides a deeper understanding of the function of RUNX3 and new insights for the treatment of related diseases. However, at present, we selected only one of the mutants, R122C, to construct overexpression cell lines to validate the experimental results. Further functional experiments with other mutations are worth performing in the future.

Host restriction factors are a powerful impediment to viral replication. As a result of long-term host-virus interactions, viruses have evolved corresponding mechanisms to antagonize restriction factors. Viral antagonists often couple restriction factors to proteasomal degradation pathways, resulting in restriction factor mislocalization or acting as restriction factor substrate analogs to influence host restriction factor action (56). Our studies show that RTA in KSHV acts as a corresponding antagonist of RUNX3, interacting with and promoting RUNX3 degradation through the proteasome pathway. Future work may also need to identify the precise ubiquitination site of RUNX3.

Most studies have demonstrated the involvement of RUNX3 as a tumor suppressor in the development of various cancers such as gastric, pancreatic, and breast cancers (28). Meanwhile, our work shows that transcriptional repression of RUNX3 severely hindered

the replication of KSHV genes and the production of progeny viral particles. It implies that RUNX3 may also act as a tumor suppressor in KSHV-induced malignancies.

In summary, our work identifies for the first time RUNX3 as a novel host restriction factor targeting KSHV lytic replication through transcriptional repression. The dynamic change in RUNX3 expression during KSHV reactivation reflects the mutual antagonism between the host and the virus as they respond to each other. In addition, the fact that RUNX3 exhibits strong antiviral capacity during the KSHV life cycle broadens our understanding of the function of RUNX3 and provides a possible mechanism for RUNX3 to play a role in other viruses. Moreover, RUNX3 is expected to be a potential target of therapeutic strategies for KSHV-related diseases.

MATERIALS AND METHODS

Cell culture

iSLK.RGB cells (a gift from Dr. Jae Jung) were cultured in Dulbecco's modified Eagle's medium (DMEM, HyClone) supplemented with 10% FBS (Biological Industries), 1% antibiotics (penicillin and streptomycin, Gibco), 10 µg/mL puromycin (Sigma), 250 µg/mL G418 (Sigma), and 250 µg/mL hygromycin B (Roche). iSLK.RGB-Vector, iSLK.RGB-RUNX3, and iSLK.RGB-R122C were generated by lentivirus-mediated transduction according to the manufacturer's instructions (System Bioscience, Palo Alto, USA) and were maintained in selection media with blasticidin (50 µg/mL). BCBL1 were cultured in RPMI 1640 (HyClone) containing 10% FBS and 1% antibiotics. HEK293T and Hela cell lines were cultured in DMEM supplemented with 10% FBS and 1% antibiotics.

Plasmid

Mammalian expression plasmids for RUNX3 and viral gene RTA were constructed by inserting the corresponding full-length fragments into PCDNA-3.1-HA and PCDH-CMV-SF-IRES-Blast vectors. The full-length fragments were generated by PCR amplification using cDNA from iSLK.RGB cells. The RUNX3-associated mutant plasmid was constructed using the PCDH-CMV-SF-RUNX3 plasmid as a template, amplified by PCR using specific mutant primers and digested by DpnI. Virus-associated luciferase reporter gene plasmids were kept for our laboratory. The sequences of the PCR amplification primers used in this study are shown in Table 1.

Antibodies and reagents

The primary antibodies were used in this study: anti-RUNX1 rabbit polyclonal antibody (ABclonal, A2055), anti-RUNX2 rabbit monoclonal antibody (ABclonal, A11753), anti-RUNX3 rabbit monoclonal antibody (Abcam, ab224641), anti-DDDDK-Tag mouse monoclonal antibody (ABclonal, AE005), anti-α-tubulin mouse monoclonal antibody (Sigma, T6199), anti-RTA rabbit monoclonal antibody (prepared in our laboratory), HA antibody (Sigma, H9658), anti-GAPDH mouse monoclonal antibody (ABclonal, AC033), anti-UBC rabbit polyclonal antibody (ABclonal, A3207), anti-BrdU mouse monoclonal antibody (ABclonal, A1482), NF-kB p65/RelA rabbit polyclonal antibody (ABclonal, A2547), and the Phospho-NF-κB p65 rabbit monoclonal antibody (CST, #3033).

The secondary antibodies were used in this study: goat anti-rabbit immunoglobulin (Jackson ImmunoResearch, 111-005-144), goat anti-mouse immunoglobulin (Jackson ImmunoResearch, 115-035-174), goat anti-rabbit-conjugated 488 (green) fluorescent antibody (Invitrogen, A 11094), goat anti-rabbit-conjugated 555 (red) fluorescent antibody (Invitrogen, A-27017), goat anti-mouse-conjugated 488 (green) fluorescent antibody (Invitrogen, A-11001), and goat anti-mouse-conjugated 555 (red) fluorescent antibody (Invitrogen, A-21422).

The reagents were used in this study: restriction endonuclease (Takara), SYBR Green Mix (Yeasen), anti-Flag M2 beads (Sigma), recombinant protein G agarose (Invitrogen), recombinant protein A agarose (Invitrogen), DAPI (Beyotime), RIPA lysate (weak)

TABLE 1 Primers for PCR amplification, qPCR, and ChIP-qPCR analysis

Primer name	Sequence of oligonucleotide (5′–3′)
CMV-SF-RUNX3-F	GATCTCGAGCTCAAGCTTCGAATTCATGCGTATTCCCGTAGACCCAAG
CMV-SF-RUNX3-R	CTTCTCGAACTGAGGGTGGCTCCAGGATCCGTAGGGCCGCCACACGG
3.1-HA-RTA-F	AGTCCAGTGTGGTGGAATTCATGGCGCAAGATGACAAGGGTA
3.1-HA-RTA-R	ACGTCGTATGGGTATCTAGAGTCTCGGAAGTAATTACGCCAT
CMV-SF-R122C-F	GACGAGAACTACTCCGCTGAGCTGTGCAATGCCTCG
CMV-SF-R122C-R	CTTCATGACGGCCGAGGCATTGCACAGCTCAGC
CMV-SF-R143Q-F	CGACCTTCGCTTCGTGGGCCAGAGTGGGCGAGGGA
CMV-SF-R143Q-R	GGTCAGGGTGAAACTCTTCCCTCGCCCACTCTGGCCCACGAAG
CMV-SF-G145E-F	CAACGACCTTCGCTTCGTGGGCCGCAGTGAGCGAGGG
CMV-SF-G145E-R	CAGGGTGAAACTCTTCCCTCGCTCACTGCGGCCCACG
CMV-SF-T151A-F	GGCCGCAGTGGGCGAGGGAAGAGTTTCGCCCTGACCATCA
CMV-SF-T151A-R	GGGGTTGGTGAACACAGTGATGGTCAGGGCGAAACTCTTCCCTCG
qPCR-K9-F	GTCTCTGCGCCATTCAAAAC
qPCR-K9-R	CCGGACACGACAACTAAGAA
qPCR-RUNX1-F	CTGCCCATCGCTTTCAAGGT
qPCR-RUNX1-R	GCCGAGTAGTTTTCATCATTGCC
qPCR-RUNX2-F	TGGTTACTGTCATGGCGGGTA
qPCR-RUNX2-R	TCTCAGATCGTTGAACCTTGCTA
qPCR-RUNX3-F	AGGCAATGACGAGAACTACTCC
qPCR-RUNX3-R	CGAAGGTCGTTGAACCTGG
qPCR-Actin-F	CATGTACGTTGCTATCCAGGC
qPCR-Actin-R	CTCCTTAATGTCACGCACGAT
qPCR-GAPDH-F	GGAGCGAGATCCCTCCAAAAT
qPCR-GAPDH-R	GGCTGTTGTCATACTTCTCATGG
qPCR-RTA-F	AGACCCGGCGTTTATTAGTACGT
qPCR-RTA-R	CAGTAATCACGGCCCCTTGA
qPCR-ORF73-F	GCAGACTACACCTCCACACT
qPCR-ORF73-R	GTAGATCGGGGACTCTGTGG
qPCR-ORF45-F	GGGATGGGTTAGTCAGGATG
qPCR-ORF45-R	CCTCGTCGTCTGAAGGTGA
qPCR-ORF57-F	TGGACATTATGAAGGGCATCCTA
qPCR-ORF57-R	CGGGTTCGGACAATTGCT
qPCR-ORF65-F	ATATGTCGCAGGCCGAATAC
qPCR-ORF65-R	CCACCCATCCTCCTCAGATA
qPCR-K8.1-F	AAAGCGTCCAGGCCACCACAGA
qPCR-K8.1-R	GGCAGAAAATGGCACACGGTTAC
qPCR-PAN-F	GCCGCTTCTGGTTTTCATTG
qPCR-PAN-R	TTGCCAAAAGCGACGCA
qPCR-P65-F	ATGTGGAGATCATTGAGCAGC
qPCR-P65-R	CCTGGTCCTGTGTAGCCATT
ChIP-qPCR-ORF73-F	CAAGGTTAAAGTGGGTTTGCTG
ChIP-qPCR-ORF73-R	GGTTATTGGCCGTTTCTGTTTC
ChIP-qPCR-K8-F	GCGTAATTACTTCCGAGACTGA
ChIP-qPCR-K8-R	TTAACTCCACTTTGCACCAAAC
ChIP-qPCR-ORF50-F	GACAGTCCGCCATACTCTTC
ChIP-qPCR-ORF50-R	CTGGCTCTACCACATCTTCATAG
ChIP-qPCR-vIRF2-F	TGCGGAAACTTGTGGTTAGA
ChIP-qPCR-vIRF2-R	GCTTGTATTAGAGGGTGGACAG
ChIP-qPCR-K7-F	CCATATTTGGTAGGAGTATGGAGTT
ChIP-qPCR-K7-R	GACAGGTTAGCCACCCATTT
ChIP-qPCR-ORF59-F	AACCGCAGTTCGTCAGGACCACCA
ChIP-qPCR-ORF59-R	CCTTAGCCACTTAAGTAGGAATG

(*Continued on next page*)

TABLE 1 Primers for PCR amplification, qPCR, and ChIP-qPCR analysis (*Continued*)

Primer name	Sequence of oligonucleotide (5′–3′)
ChIP-qPCR-ORF25-F	GTTAGTAGCGCGGGAAGATAC
ChIP-qPCR-ORF25-R	GACAGATAGACACCGACAACTAC
ChIP-qPCR-ORF63-F	GGGTGTTAGCAGCATATCCATAG
ChIP-qPCR-ORF63-R	CCTCGTGTATTCACAGACCTTTAG

(Beyotime), Trizol (Invitrogen), nitrocellulose membranes (Pall Corporation, USA), 10 × DNA loading buffer (Takara), ECL substrate luminescence color development kit (Millipore), Tween 20 (Sigma), Opti-MEM and Lipo2000 (Invitrogen), BrdU (MedChemExpress) BAY-7082 (MedChemExpress), BX795 (MedChemExpress), Dox (Sigma-Aldrich), TPA (Sigma-Aldrich), CHX (MedChemExpress, HY-12320), and MG132 (MedChemExpress, HY-13259).

Western blot and Co-IP

In immunoblotting experiments, cells after 48 h of transfection were lysed in Western and IP lysate (Beyotime) containing 1 mM PMSF and protease inhibitor cocktail. After 30 min, they were mixed with 5× SDS gel loading buffer and separated by SDS-PAGE electrophoresis. For Co-IP, cells were lysed in Western and IP lysates for 30 min and then centrifuged to remove cell debris. A portion of the lysate was taken as input and the remaining lysate was incubated overnight with anti-Flag antibody or anti-RTA antibody. After three washes of lysis buffer, the lysates were resuspended using 2× SDS gel loading buffer, followed by SDS-PAGE electrophoretic separation and transfer to nitrocellulose membranes, which were incubated with the indicated primary antibodies and HRP-conjugated secondary antibodies, and then visualized with ECL reagent (GE).

RNA isolation and quantitative real-time PCR

Cells were lysed using TRIzol reagent (Invitrogen) and total RNA was extracted according to the reagent vendor's instructions. Two microgram of RNA was taken for reverse transcription with HiScript III RT SuperMix (Vazyme, R323-01). RT-qPCR was performed on QuantStudio 6 Flex Real-Time PCR System (Applied Biosystems) using a Hieff qPCR SYBR Green Master Mix (YEASEN, 11202ES03) with cDNA as template. Transcript levels of each gene were normalized to the GAPDH level, and the $2^{-\Delta\Delta CT}$ method was used to analyze gene expression in samples. Data represent fold changes compared to the level for control groups. The primers used for RT-qPCR are shown in Table 1.

RNA interference

Two siRNA oligonucleotides targeting human RUNX3 or P65 and negative control siRNA were ordered from GenePharma. These siRNAs were transfected into iSLK.RGB cells by Lipofectamine 2000 following the manufacturer's instructions. All siRNA sequences used in the experiments are listed below:

Negative control siRNA, 5′-ACGUGACACGUUCGGAGAATT-3′; siRUNX3#1, 5′-AAGCGAAGGUCGUUGAACCTT-3′; siRUNX3#2, 5′-AAUGGGUUCAGUUCCGAGGTT-3′;

Negative control siRNA, 5′-ACGUGACACGUUCGGAGAATT-3′ siP65#1, 5′-UCAUCAUAGUUGAUGGUGCTT-3′; siP65#2, 5′-UAUAGCCUCAGGGUACUCCTT-3′.

Dual-luciferase reporter assay

HEK293T cells are grown in 12-well plates at the appropriate density (~5 × 10^5). The next day cells were transfected with the indicated luciferase reporter plasmids (25 ng pRL-TK, 1 µg PGL3-ORF57/ORF59/PAN/K8.1) and protein expression plasmids (0.3 µg RTA-HA, increasing 0, 0.1, 0.3 µg RUNX3-Flag, 0.3 µg RUNX3/R122C/R143Q/G145E/DM/T151A-Flag). After 48 h of transfection, cells were lysed with 200 µL of 1 × passive lysis buffer at room temperature for 20 min, and 10 µL of the lysate was taken to detect

luciferase activity using the Dual Luciferase Reporter Assay System (Promega) according to the manufacturer's instructions. In this experiment, the plasmid expressing Renilla luciferase was used to normalize firefly luciferase activity.

KSHV virus production and infection assays

iSLK.RGB cells and their modified cell lines grown in 6-well plates (~1×10^6) were treated with Dox. After 48 h of induction, supernatants from each group were collected and centrifuged to remove cellular debris. Then, 1 mL of new supernatant was then removed and used to infect HEK293T cells grown in 12-well plates (~5×10^5) by centrifugation at 37°C and 2,500 rpm for 2 h. After infection, the viral supernatant was discarded and replaced with fresh DMEM to continue the culture.

Immunofluorescence assay and BrdU

HeLa cells were cultivated onto coverslips in 24-well plates and transfected with the indicated plasmids. After 24 h of transfection, cells were washed three times with PBS and fixed in 4% paraformaldehyde for 30 min. Cells were permeabilized with 0.1% Triton X-100 for 20 min and blocked with 1% bovine serum albumin (BSA) for 60 min and then incubated with specific primary antibody (1:200 dilution) overnight at 4°C. After being washed six times with PBS, cells were incubated with fluorescent secondary antibody (1:200 dilution) for 60 min at room temperature avoiding light. Cell nuclei were stained with DAPI (1:1,000 dilution) for 5 min. Finally, coverslips were rinsed five times and fixed on slides. The slides were analyzed with a DM6000B fluorescence microscope (Leica, Inc., Solms, Germany) for observation and photography.

For BrdU insertion experiments, we treated BCBL1 cells with TPA and NaB for 24 h and then replaced the culture medium with DMEM containing 10 µM BrdU. Incubation at 37°°C for 2 h was followed by centrifugation, and the cells were resuspended with PBS. Then, the cell suspension was dripped onto polylysine-adherent slides (Solarbio). After the liquid dried naturally, the cells were fixed with 4% formaldehyde for 30 min at room temperature and subsequently permeabilized with 0.1% Triton X-100 for 20 min at room temperature. After removal of the permeabilization buffer, cells were incubated on ice with 1 M HCl for 10 min and with 2 M HCl for 10 min at room temperature. Cells were rinsed three times with PBS and then neutralized with 0.1 M sodium borate buffer for 30 min at room temperature. After washing with Triton X-100 permeabilization buffer, cells were incubated overnight at 4°C with primary anti-BrdU and anti-RUNX3 antibodies. The following steps were the same as described above.

Chromatin immunoprecipitation

BeyoChIP Enzymatic ChIP Assay Kit (Beyotime, P2083S) was used for this experiment, and the operation was performed according to the manufacturer's instructions. The iSLK.RGB cells were induced by Dox, or BCBL1 cells were induced by TPA for 48 h. Appropriate amount of formaldehyde was added to a final concentration of 1%, followed by cross-linking by incubation at 37°C for 10 min. Crosslinking was terminated by adding 1.1 mL of Glycine Solution (10×) and left at room temperature for 5 min. After washing the cells twice with cold PBS, the cells were resuspended in 1 mL PBS for subsequent nucleocytoplasmic separation. The nucleus extract was added with 1 µL of MNase and incubated at 37°C for 20 min. The MNase fragmentation reaction was terminated by adding 10 µL of 0.5 M EDTA to the mixture placed on ice for 2 min. Chromatin was then further fragmented using a Bioruptor Pico sonicator (10 s per sonication at 30 s intervals for three times). A 10 µL sample was taken to reverse crosslinks and then subjected to agarose gel electrophoresis to ensure that the fragment size was between 200 bp and 800 bp. The remaining sample was centrifuged at 13,000×*g* for 5 min at 4°C. The supernatant was added to the ChIP Buffer to a final volume of 0.5 mL, 10 µL of the sample was removed as 2% Input, and the remaining sample was incubated with the appropriate amount of primary antibody at 4°C overnight. The next day 30 µL of Protein

A/G Magnetic Beads/Salmon Sperm DNA was added to the samples and mixed for 60 min at 4°C with rotation. Sequentially washed once in low salt buffer, high salt buffer, LiCl buffer and twice in TE buffer. Finally, the complex was eluted in 300 µL of Elution buffer and subjected to reverse crosslinks and DNA purification. ChIP-enriched DNA was quantified by real-time quantitative PCR (qPCR) using a Hieff qPCR SYBR Green Master Mix and the primers listed in Table 1. Protein enrichment on specific genomic regions was calculated as fold enrichment relative to control IgG ChIP.

Protein stability assay

HEK293T cells were transfected with the indicated plasmids. After 24 h of transfection, cells were treated with 100 µg/mL CHX to inhibit protein synthesis. Cells were collected at the indicated time points and lysed for immunoblot analysis. The intensity of each RUNX3 band was normalized to the GAPDH protein intensity and then compared with RUNX3 at 0 h.

Ubiquitination assay

The indicated plasmids were co-transfected with HEK293T cells for 24 h and then switched to DMEM containing MG132 (20 µM) or DMSO for 12 h. The cells were then lysed and immunoprecipitated with an anti-Flag M2 affinity gel. After overnight incubation, the cells were analyzed by immunoblotting with anti-UBC rabbit polyclonal antibody.

Statistical analysis

The statistical analysis was performed by using the unpaired student's *t* tests or student's multiple *t* tests in GraphPad Prism 8. Data were shown as mean ± SD (error bars) from at least three independent experiments and statistical significance was set as *P*-value < 0.05.

ACKNOWLEDGMENTS

This work was supported by the grants from Natural Science Foundation of China (32188101, 81930060) to K.L.

AUTHOR AFFILIATIONS

[1]State Key Laboratory of Virology, College of Life Sciences, Wuhan University, Wuhan, China
[2]Department of Infectious Diseases, Frontier Science Center for Immunology and Metabolism, Medical Research Institute, Zhongnan Hospital of Wuhan University, Wuhan University, Wuhan, China
[3]Taikang Center for Life and Medical Sciences, Wuhan University, Wuhan, China

AUTHOR ORCIDs

Pengyu Ren http://orcid.org/0009-0003-3965-7173
Ke Lan http://orcid.org/0000-0002-0384-8598

AUTHOR CONTRIBUTIONS

Pengyu Ren, Data curation, Formal analysis, Investigation, Methodology, Project administration, Validation, Visualization, Writing – original draft, Writing – review and editing | Danping Niu, Conceptualization, Methodology, Resources, Software, Supervision, Writing – review and editing | Sijia Chang, Methodology, Resources, Supervision | Lei Yu, Methodology, Resources, Software | Junrui Ren, Resources, Validation | Yuanming Ma, Validation | Ke Lan, Conceptualization, Formal analysis, Funding acquisition, Project administration, Supervision, Writing – review and editing

ADDITIONAL FILES

The following material is available online.

Supplemental Material

Supplemental figure (JVI01567-23-s0001.pdf). Figure S1.

REFERENCES

1. Chang Y, Cesarman E, Pessin MS, Lee F, Culpepper J, Knowles DM, Moore PS. 1994. Identification of herpesvirus-like DNA sequences in AIDS-associated Kaposi's sarcoma. Science 266:1865–1869. https://doi.org/10.1126/science.7997879
2. Cesarman E, Chadburn A, Rubinstein PG. 2022. KSHV/HHV8-mediated hematologic diseases. Blood 139:1013–1025. https://doi.org/10.1182/blood.2020005470
3. Bhutani M, Polizzotto MN, Uldrick TS, Yarchoan R. 2015. Kaposi sarcoma–associated herpesvirus-associated malignancies: epidemiology, pathogenesis, and advances in treatment. Semin Oncol 42:223–246. https://doi.org/10.1053/j.seminoncol.2014.12.027
4. Ye F, Lei X, Gao S-J. 2011. Mechanisms of Kaposi's sarcoma-associated herpesvirus latency and reactivation. Adv Virol 2011:193860. https://doi.org/10.1155/2011/193860
5. Cotter MA II, Robertson ES. 1999. The latency-associated nuclear antigen tethers the Kaposi's sarcoma-associated herpesvirus genome to host chromosomes in body cavity-based lymphoma cells. Virology 264:254–264. https://doi.org/10.1006/viro.1999.9999
6. Barbera AJ, Chodaparambil JV, Kelley-Clarke B, Joukov V, Walter JC, Luger K, Kaye KM. 2006. The nucleosomal surface as a docking station for Kaposi's sarcoma herpesvirus LANA. Science 311:856–861. https://doi.org/10.1126/science.1120541
7. Mesri EA, Cesarman E, Boshoff C. 2010. Kaposi's sarcoma and its associated herpesvirus. Nat Rev Cancer 10:707–719. https://doi.org/10.1038/nrc2888
8. Friborg J, Kong W, Hottiger MO, Nabel GJ. 1999. P53 inhibition by the LANA protein of KSHV protects against cell death. Nature 402:889–894. https://doi.org/10.1038/47266
9. Lan K, Kuppers DA, Verma SC, Robertson ES. 2004. Kaposi's sarcoma-associated herpesvirus-encoded latency-associated nuclear antigen inhibits lytic replication by targeting RTA: a potential mechanism for virus-mediated control of latency. J Virol 78:6585–6594. https://doi.org/10.1128/JVI.78.12.6585-6594.2004
10. Juillard F, Tan M, Li S, Kaye KM. 2016. Kaposi's sarcoma herpesvirus genome persistence. Front Microbiol 7:1149. https://doi.org/10.3389/fmicb.2016.01149
11. Li T, Gao S-J. 2023. KSHV hijacks FoxO1 to promote cell proliferation and cellular transformation by antagonizing oxidative stress. J Med Virol 95:e28676. https://doi.org/10.1002/jmv.28676
12. Gramolelli S, Schulz TF. 2015. The role of Kaposi sarcoma-associated herpesvirus in the pathogenesis of Kaposi sarcoma. J Pathol 235:368–380. https://doi.org/10.1002/path.4441
13. Coen N, Duraffour S, Snoeck R, Andrei G. 2014. KSHV targeted therapy: an update on inhibitors of viral lytic replication. Viruses 6:4731–4759. https://doi.org/10.3390/v6114731
14. Zhu X, Guo Y, Yao S, Yan Q, Xue M, Hao T, Zhou F, Zhu J, Qin D, Lu C. 2014. Synergy between Kaposi's sarcoma-associated herpesvirus (KSHV) vIL-6 and HIV-1 Nef protein in promotion of angiogenesis and oncogenesis: role of the AKT signaling pathway. Oncogene 33:1986–1996. https://doi.org/10.1038/onc.2013.136
15. Davis DA, Rinderknecht AS, Zoeteweij JP, Aoki Y, Read-Connole EL, Tosato G, Blauvelt A, Yarchoan R. 2001. Hypoxia induces lytic replication of Kaposi sarcoma-associated herpesvirus. Blood 97:3244–3250. https://doi.org/10.1182/blood.v97.10.3244
16. Gradoville L, Gerlach J, Grogan E, Shedd D, Nikiforow S, Metroka C, Miller G. 2000. Kaposi's sarcoma-associated herpesvirus open reading frame 50/RTA protein activates the entire viral lytic cycle in the HH-B2 primary effusion lymphoma cell line. J Virol 74:6207–6212. https://doi.org/10.1128/jvi.74.13.6207-6212.2000
17. Yu Y, Wang SE, Hayward GS. 2005. The KSHV immediate-early transcription factor RTA encodes ubiquitin E3 ligase activity that targets IRF7 for proteosome-mediated degradation. Immunity 22:59–70. https://doi.org/10.1016/j.immuni.2004.11.011
18. Yu Y, Hayward GS. 2010. The ubiquitin E3 ligase RAUL negatively regulates type I interferon through ubiquitination of the transcription factors IRF7 and IRF3. Immunity 33:863–877. https://doi.org/10.1016/j.immuni.2010.11.027
19. Ehrlich ES, Chmura JC, Smith JC, Kalu NN, Hayward GS. 2014. KSHV RTA abolishes NFκB responsive gene expression during lytic reactivation by targeting vFLIP for degradation via the proteasome. PLoS One 9:e91359. https://doi.org/10.1371/journal.pone.0091359
20. Yang Z, Yan Z, Wood C. 2008. Kaposi's sarcoma-associated herpesvirus transactivator RTA promotes degradation of the repressors to regulate viral lytic replication. J Virol 82:3590–3603. https://doi.org/10.1128/JVI.02229-07
21. Zhao Q, Liang D, Sun R, Jia B, Xia T, Xiao H, Lan K, Hutt-Fletcher LM. 2015. Kaposi's sarcoma-associated herpesvirus-encoded replication and transcription activator impairs innate immunity via ubiquitin-mediated degradation of myeloid differentiation factor 88. J Virol 89:415–427. https://doi.org/10.1128/JVI.02591-14
22. Han C, Zhang D, Gui C, Huang L, Chang S, Dong L, Bai L, Wu S, Lan K, Dittmer DP. 2022. KSHV RTA antagonizes SMC5/6 complex-induced viral chromatin compaction by hijacking the ubiquitin-proteasome system. PLoS Pathog 18:e1010744. https://doi.org/10.1371/journal.ppat.1010744
23. Ito Y. 2004. Oncogenic potential of the RUNX gene family: 'overview' Oncogene 23:4198–4208. https://doi.org/10.1038/sj.onc.1207755
24. Tahirov TH, Inoue-Bungo T, Morii H, Fujikawa A, Sasaki M, Kimura K, Shiina M, Sato K, Kumasaka T, Yamamoto M, Ishii S, Ogata K. 2001. Structural analyses of DNA recognition by the AML1/RUNX-1 runt domain and its allosteric control by CBFbeta. Cell 104:755–767. https://doi.org/10.1016/s0092-8674(01)00271-9
25. Bangsow C, Rubins N, Glusman G, Bernstein Y, Negreanu V, Goldenberg D, Lotem J, Ben-Asher E, Lancet D, Levanon D, Groner Y. 2001. The RUNX3 gene--sequence, structure and regulated expression. Gene 279:221–232. https://doi.org/10.1016/s0378-1119(01)00760-0
26. Lacaud G, Gore L, Kennedy M, Kouskoff V, Kingsley P, Hogan C, Carlsson L, Speck N, Palis J, Keller G. 2002. Runx1 is essential for hematopoietic commitment at the hemangioblast stage of development *in vitro*. Blood 100:458–466. https://doi.org/10.1182/blood-2001-12-0321
27. Fujita T, Azuma Y, Fukuyama R, Hattori Y, Yoshida C, Koida M, Ogita K, Komori T. 2004. Runx2 induces osteoblast and chondrocyte differentiation and enhances their migration by coupling with PI3K-Akt signaling. J Cell Biol 166:85–95. https://doi.org/10.1083/jcb.200401138
28. Chuang LSH, Ito Y. 2010. RUNX3 is multifunctional in carcinogenesis of multiple solid tumors. Oncogene 29:2605–2615. https://doi.org/10.1038/onc.2010.88
29. Koh CP, Wang CQ, Ng CEL, Ito Y, Araki M, Tergaonkar V, Huang G, Osato M. 2013. RUNX1 meets MLL: epigenetic regulation of hematopoiesis by two leukemia genes. Leukemia 27:1793–1802. https://doi.org/10.1038/leu.2013.200
30. Ellis MJ, Ding L, Shen D, Luo J, Suman VJ, Wallis JW, Van Tine BA, Hoog J, Goiffon RJ, Goldstein TC, et al. 2012. Whole-genome analysis informs breast cancer response to aromatase inhibition. Nature 486:353–360. https://doi.org/10.1038/nature11143
31. Li QL, Ito K, Sakakura C, Fukamachi H, Inoue K ichi, Chi XZ, Lee KY, Nomura S, Lee CW, Han SB, et al. 2002. Causal relationship between the loss of RUNX3 expression and gastric cancer. Cell 109:113–124. https://doi.org/10.1016/s0092-8674(02)00690-6
32. Hu Y, Pan Q, Zhou K, Ling Y, Wang H, Li Y. 2022. RUNX1 inhibits the antiviral immune response against influenza A virus through attenuating type I interferon signaling. Virol J 19:39. https://doi.org/10.1186/s12985-022-01764-8

33. Gan H, Hao Q, Idell S, Tang H. 2015. Transcription factor RUNX3 is induced by influenza A virus and double-strand RNA and mediates airway epithelial cell apoptosis. Sci Rep 5:17916. https://doi.org/10.1038/srep17916
34. Kim DJ, Khoury-Hanold W, Jain PC, Klein J, Kong Y, Pope SD, Ge W, Medzhitov R, Iwasaki A. 2020. RUNX binding sites are enriched in herpesvirus genomes, and RUNX1 overexpression leads to herpes simplex virus 1 suppression. J Virol 94:e00943-20. https://doi.org/10.1128/JVI.00943-20
35. Gunnell A, Webb HM, Wood CD, McClellan MJ, Wichaidit B, Kempkes B, Jenner RG, Osborne C, Farrell PJ, West MJ. 2016. RUNX super-enhancer control through the notch pathway by Epstein-Barr virus transcription factors regulates B cell growth. Nucleic Acids Res 44:4636–4650. https://doi.org/10.1093/nar/gkw085
36. Spender LC, Whiteman HJ, Karstegl CE, Farrell PJ. 2005. Transcriptional cross-regulation of RUNX1 by RUNX3 in human B cells. Oncogene 24:1873–1881. https://doi.org/10.1038/sj.onc.1208404
37. Brulois K, Toth Z, Wong LY, Feng P, Gao SJ, Ensser A, Jung JU. 2014. Kaposi's sarcoma-associated herpesvirus K3 and K5 ubiquitin E3 ligases have stage-specific immune evasion roles during lytic replication. J Virol 88:9335–9349. https://doi.org/10.1128/JVI.00873-14
38. Myoung J, Ganem D. 2011. Generation of a doxycycline-inducible KSHV producer cell line of endothelial origin: maintenance of tight latency with efficient reactivation upon induction. J Virol Methods 174:12–21. https://doi.org/10.1016/j.jviromet.2011.03.012
39. Miller G, Heston L, Grogan E, Gradoville L, Rigsby M, Sun R, Shedd D, Kushnaryov VM, Grossberg S, Chang Y. 1997. Selective switch between latency and lytic replication of Kaposi's sarcoma herpesvirus and Epstein-Barr virus in dually infected body cavity lymphoma cells. J Virol 71:314–324. https://doi.org/10.1128/jvi.71.1.314-324.1997
40. Gan H, Hao Q, Idell S, Tang H. 2016. Interferon-γ promotes double-stranded RNA-induced TLR3-dependent apoptosis via upregulation of transcription factor RUNX3 in airway epithelial cells. Am J Physiol Lung Cell Mol Physiol 311:L1101–L1112. https://doi.org/10.1152/ajplung.00278.2016
41. Yano T, Ito K, Fukamachi H, Chi X-Z, Wee H-J, Inoue K, Ida H, Bouillet P, Strasser A, Bae S-C, Ito Y. 2006. The RUNX3 tumor suppressor upregulates bim in gastric epithelial cells undergoing transforming growth factor beta-induced apoptosis. Mol Cell Biol 26:4474–4488. https://doi.org/10.1128/MCB.01926-05
42. Chi XZ, Yang JO, Lee KY, Ito K, Sakakura C, Li QL, Kim HR, Cha EJ, Lee YH, Kaneda A, Ushijima T, Kim WJ, Ito Y, Bae SC. 2005. RUNX3 suppresses gastric epithelial cell growth by inducing p21(WAF1/Cip1) expression in cooperation with transforming growth factor {beta}-activated SMAD. Mol Cell Biol 25:8097–8107. https://doi.org/10.1128/MCB.25.18.8097-8107.2005
43. Ansari MA, Dutta S, Veettil MV, Dutta D, Iqbal J, Kumar B, Roy A, Chikoti L, Singh VV, Chandran B. 2015. Herpesvirus genome recognition induced acetylation of nuclear IFI16 is essential for its cytoplasmic translocation, inflammasome and IFN-beta responses. PLoS Pathog 11:e1005019. https://doi.org/10.1371/journal.ppat.1005019
44. Qiao Y, Lin SJ, Chen Y, Voon DC-C, Zhu F, Chuang LSH, Wang T, Tan P, Lee SC, Yeoh KG, Sudol M, Ito Y. 2016. RUNX3 is a novel negative regulator of oncogenic TEAD-YAP complex in gastric cancer. Oncogene 35:2664–2674. https://doi.org/10.1038/onc.2015.338
45. Kim J-H, Jang J-W, Lee Y-S, Lee J-W, Chi X-Z, Li Y-H, Kim M-K, Kim D-M, Choi B-S, Kim J, Kim H-M, van Wijnen A, Park I, Bae S-C. 2014. RUNX family members are covalently modified and regulated by PIAS1-mediated sumoylation. Oncogenesis 3:e101–e101. https://doi.org/10.1038/oncsis.2014.15
46. Chmura JC, Herold K, Ruffin A, Atuobi T, Fabiyi Y, Mitchell AE, Choi YB, Ehrlich ES. 2017. The itch ubiquitin ligase is required for KSHV RTA induced vFLIP degradation. Virology 501:119–126. https://doi.org/10.1016/j.virol.2016.11.016
47. Qiao Y, Lin SJ, Chen Y, Voon DCC, Zhu F, Chuang LSH, Wang T, Tan P, Lee SC, Yeoh KG, Sudol M, Ito Y. 2016. RUNX3 is a novel negative regulator of oncogenic TEAD–YAP complex in gastric cancer. Oncogene 35:2664–2674. https://doi.org/10.1038/onc.2015.338
48. Edelman DC. 2005. Human herpesvirus 8--a novel human pathogen. Virol J 2:78. https://doi.org/10.1186/1743-422X-2-78
49. He M, Cheng F, da Silva SR, Tan B, Sorel O, Gruffaz M, Li T, Gao S-J. 2019. Molecular biology of KSHV in relation to HIV/AIDS-associated oncogenesis. Cancer Treat Res 177:23–62. https://doi.org/10.1007/978-3-030-03502-0_2
50. Grundhoff A, Ganem D. 2004. Inefficient establishment of KSHV latency suggests an additional role for continued lytic replication in kaposi sarcoma pathogenesis. J Clin Invest 113:124–136. https://doi.org/10.1172/JCI17803
51. Aneja KK, Yuan Y. 2017. Reactivation and lytic replication of Kaposi's sarcoma-associated herpesvirus: an update. Front Microbiol 8:613. https://doi.org/10.3389/fmicb.2017.00613
52. Ma Z, Jacobs SR, West JA, Stopford C, Zhang Z, Davis Z, Barber GN, Glaunsinger BA, Dittmer DP, Damania B. 2015. Modulation of the cGAS-STING DNA sensing pathway by gammaherpesviruses. Proc Natl Acad Sci U S A 112:E4306–15. https://doi.org/10.1073/pnas.1503831112
53. West JA, Wicks M, Gregory SM, Chugh P, Jacobs SR, Zhang Z, Host KM, Dittmer DP, Damania B, Longnecker RM. 2014. An important role for mitochondrial antiviral signaling protein in the Kaposi's sarcoma-associated herpesvirus life cycle. J Virol 88:5778–5787. https://doi.org/10.1128/JVI.03226-13
54. Inoue K, Ozaki S, Shiga T, Ito K, Masuda T, Okado N, Iseda T, Kawaguchi S, Ogawa M, Bae S-C, Yamashita N, Itohara S, Kudo N, Ito Y. 2002. RUNX3 controls the axonal projection of proprioceptive dorsal root ganglion neurons. Nat Neurosci 5:946–954. https://doi.org/10.1038/nn925
55. Woolf E, Xiao C, Fainaru O, Lotem J, Rosen D, Negreanu V, Bernstein Y, Goldenberg D, Brenner O, Berke G, Levanon D, Groner Y. 2003. RUNX3 and RUNX1 are required for CD8 T cell development during thymopoiesis. Proc Natl Acad Sci U S A 100:7731–7736. https://doi.org/10.1073/pnas.1232420100
56. Duggal NK, Emerman M. 2012. Evolutionary conflicts between viruses and restriction factors shape immunity. Nat Rev Immunol 12:687–695. https://doi.org/10.1038/nri3295